Embedded Passivated-electrode Insulator-based Dielectrophoresis (EπDEP)

Tyler Joseph Shake

Thesis submitted to the faculty of the Virginia Polytechnic Institute and State University in partial fulfillment of the requirements for the degree of

Master of Science
In
Electrical Engineering

Masoud Agah, Chair

Dong S. Ha

Yizheng Zhu

March 17, 2014
Blacksburg, VA

Keywords: Dielectrophoresis (DEP), *Escherichia coli (E. coli)*, *Staphyloccus aureus (S. aureus)*, Microfluidic, Microfabrication, Insulator-based dielectrophoresis (iDEP)

Embedded Passivated-electrode Insulator-based Dielectrophoresis (EπDEP)

Tyler Joseph Shake

ABSTRACT

Pathogens in drinking water are the cause of over 1.5 million deaths around the world every year, mostly in developing countries. Practical, cheap, and effective tools for detection of these pathogens are critical to advance public health in many areas around the globe. Micro electro-mechanical systems (MEMS) are miniaturized structures that can be used for a variety of purposes, including, but not limited to, small scale sensors. Therefore, MEMS can be used in place of expensive laboratory equipment and offer a cheap and practical tool for pathogen detection.

The presented work's research objective is to introduce a new technique called embedded passivated-electrode insulator-based dielectrophoresis (EπDEP) for preconcentration, separation, or enrichment of bioparticles, including living cells. This new method combines traditional electrode-based DEP and insulator-based DEP with the objective of enhancing the electric field strength and capture efficiency within the microfluidic channel while alleviating direct contact between the electrode and the fluid. The EπDEP chip contains embedded electrodes within the microfluidic channel covered by a thin passivation layer of only 4 μm. The channel was designed with two nonaligned vertical columns of insulated microposts (200 μm diameter, 50 μm spacing) located between the electrodes (600 μm wide, 600 μm horizontal spacing) to generate the nonuniform electric field lines to concentrate cells while maintaining steady flow in the channel. The performance of the chip was demonstrated using Gram-negative (*Escherichia coli)* and Gram-positive *(Staphylococcus aureus)* bacterial pathogens in aqueous media. Trapping efficiencies of 100% were obtained for both pathogens at an applied AC voltage of 50 V peak-to-peak and flow rates as high as 10 uL/min.

This work is dedicated to my friends and family. Without the support of my father, Joe, and my mother, Tina, I would not have been able to achieve what I have today.

Acknowledgements

My deepest gratitude to:

- Dr. Masoud Agah, my advisor, who taught and guided me throughout my research.
- Dr. Amy Pruden and Dr. Bahereh Behkam for providing the cells necessary to conduct my research.
- Dr. Phillip Zellner, my mentor, who introduced and guided me throughout this endeavor.
- Dr. Ha and Dr. Zhu for serving on my thesis committee.
- Mr. Yahya Hosseini, Mr. Shree Narayanan, Ms. Vaishnavi Srinivasaraghavan, Mr. Hamza Shakeel, My Hesam Babohosseini, and Mr. Mohammad Akbar for their support and conversation within the VT MEMS Lab.

Table of Contents

List of Figures

Chapter 1

Chapter 2

Chapter 3

Chapter 4

Chapter 5

Appendix

List of Tables

1. Introduction

1.1 Background and Significance

Water-borne pathogens are the direct cause of over 1.5 million deaths world-wide every year [1]. Shown in Figure 1, Diarrhoeal diseases account for 39% of the disease burden related to hygiene, water, and sanitation. Diarrhoeal diseases are those caused by the direct ingestion of pathogens, whether through contaminated food or drinking water. Of these diseases, 88% are attributed to unsafe water causing roughly 1.5 million deaths every year, predominantly in children [2].

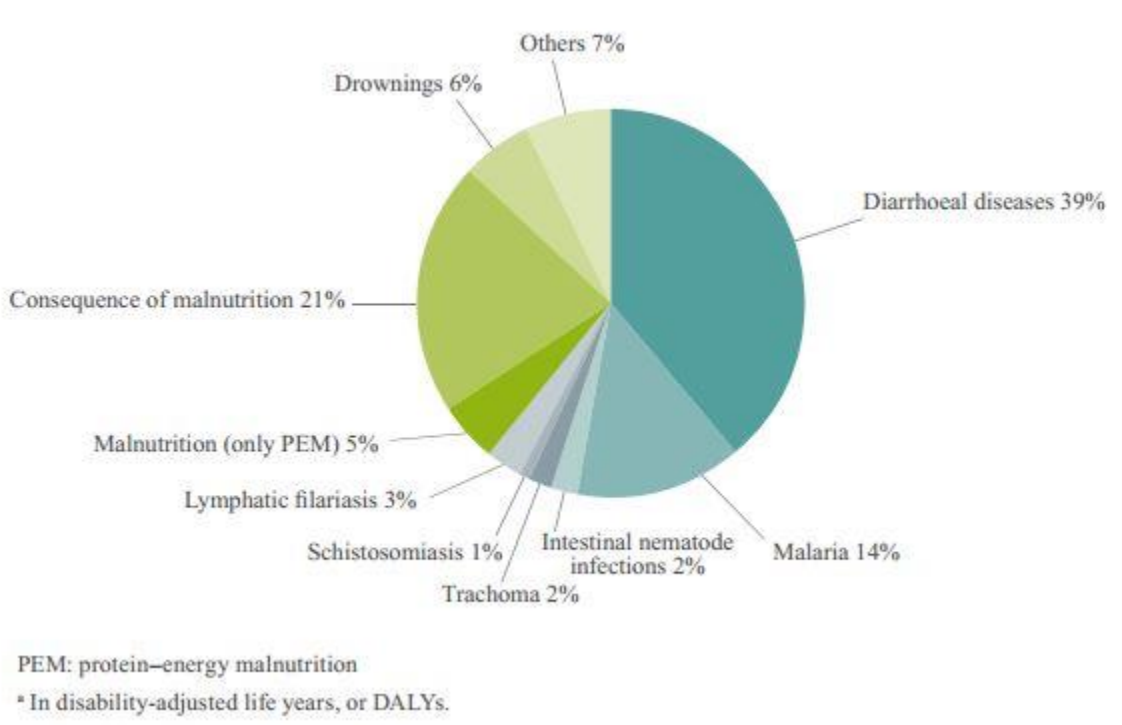

Figure 1 Diseases contributing to the water, sanitation, and hygiene-related disease burden. Pruss-Ustun, Annette, R. Bos, F. Gore, J. Bartram. "Safer Water, Better Health: Costs, benefits, and sustainability of interventions to protect and promote health." *World Health Organization*, Geneva, 2008. http://whqlibdoc.who.int/publications/2008/9789241596435_eng.pdf Used under fair use, 2014.

Current laboratory equipment to detect these biological organisms is expensive and not practical to be deployed and utilized in a significant portion of the globe. A cheap and practical solution is desired to detect these deadly pathogens within the drinking supply in developing countries around the world.

Micro electro-mechanical systems (MEMS) are miniaturized structures that can be used for a variety of purposes, including, but not limited to, small scale sensors. Therefore, MEMS can be used in place of expensive laboratory equipment and offer a cheap and practical tool for pathogen detection [3]. This goal of using MEMS to achieve micro total analysis systems (μTAS), replacing expensive and large laboratory equipment, has sparked much interest in researchers. Besides the practicality of MEMS, a large driving force is the change in influence of different physical factors that have been studied for years. For example, in large scale physics (meters), inertia and gravity are significant forces while surface tension and electrostatic forces are minute. However, in small scale physics (microns), surface tension and electrostatic forces are significant while inertia and gravity are negligible. Another significant force on the micron level that is the subject of much research today is dielectrophoresis (DEP).

1.2 Dielectrophoresis

Dielectrophoresis is a well-known electric field technique for separating, trapping, and manipulating micro and nanoparticles [4]. DEP is the movement of a particle in a nonuniform electric field due to the interaction between the electric field gradient and the particle dipole [5]. DEP has been proven useful in the characterization of biological cells due to their small sizes (~1–10 μm). DEP also provides many independent variables to utilize in order to manipulate particles including signal frequency, signal magnitude, and electrode spacing, as well as the ability to produce both positive and negative forces. Because of this, DEP has been shown to be

an effective technique in manipulating a wide range of biological particles including bacteria [6], proteins [7], viruses [8], and yeast [9].

Traditionally, two means have been used to generate the necessary nonuniform electric fields for producing a DEP force: electrode-based DEP devices (eDEP) and insulator-based DEP devices (iDEP). eDEP and iDEP technologies are shown schematically in Figure 2.

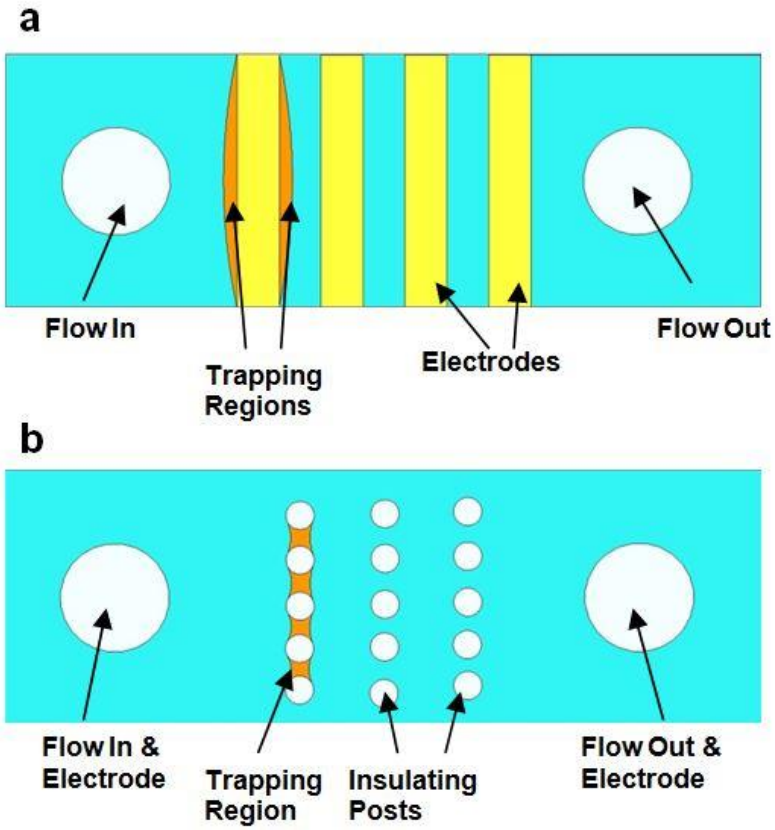

Figure 2 Example of eDEP and iDEP functionality. (a) eDEP design consisting of rectangular electrodes with trapping regions shown (b) iDEP design consisting of circular insulating posts with trapping regions shown

eDEP devices create nonuniform fields with various electrode design shapes and spacings [10,11]. An example of an electrode design shaped to produce nonuniform electric fields is shown in Figure 2(a). eDEP devices are advantageous in that they allow flexibility in electrode shape design. However, because the location of the highest magnitude of electric field gradient is near the electrodes [12], the devices will decline in performance as more particles are trapped, creating a further separation between the particles and the electrodes. Also, eDEP devices require electrodes to directly contact the solution, which could lead to gas evolution and compromise sample purity [13]. Alternatively, iDEP devices use insulating structures to produce nonuniform electric fields to drive DEP forces. An example of iDEP is shown in Figure 2(b). The electric field is applied throughout the channel, and the nonuniform electric fields are created by the insulating structures. iDEP devices are advantageous by allowing flexible insulating structure designs while also avoiding electrode fouling typical in eDEP devices. Figure 3 highlights various insulator shapes and designs found in DEP literature. The typical application of the electric field throughout the channel in iDEP devices, however, leads to a large heat buildup and Joule heating effects near the insulating structures [13]. The electrodes also must contact the solution in conventional iDEP devices, potentially leading to similar eDEP problems of gas evolution and compromising sample purity.

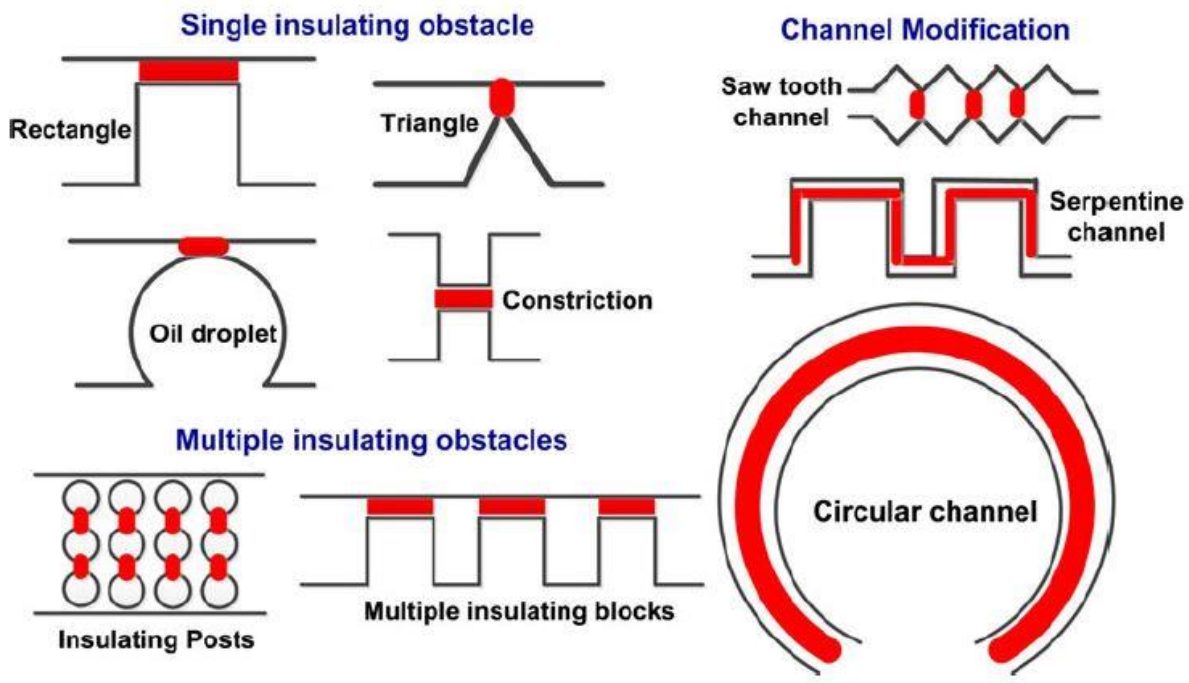

Figure 3 Different types of insulating designs found in literature. Srivastava, Soumya K, A. Gencoglu, A. R. Minerick. "DC insulator dielectrophoretic applications in microdevice technology: a review." *Analytical and Bioanalytical Chemistry*. 2010. Used under fair use, 2014.

In this work, a new DEP technique is introduced by combining the advantages of iDEP and eDEP devices. Embedded passivated-electrode insulator-based dielectrophoresis (EπDEP) chips are designed to achieve high efficiency trapping at low voltages while being scalable in terms of throughput. The schematic of the EπDEP chip is shown in Figure 4 and a photograph of the fabricated device is shown in Figure 5.

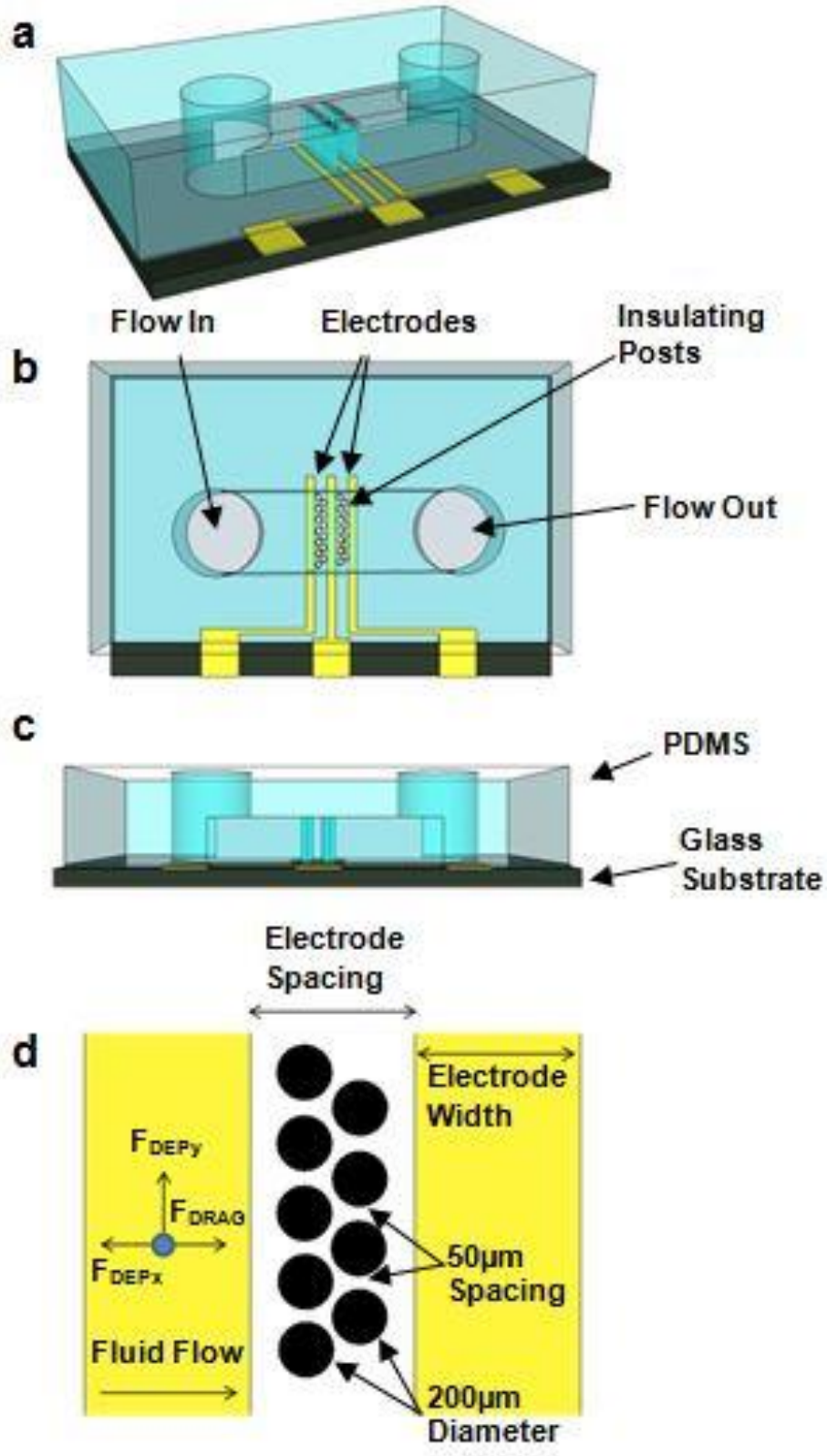

Figure 4 Schematic of EπDEP device. (a) Isometric view (b) Top view displaying electrode alignment (c) Front view showing material composition (d) Close-up view of the functional region of the device

The embedded electrodes are flexible in design shape and have the ability to produce strong electric fields within the channel, but avoid the pitfalls of typical eDEP devices by capacitive coupling the electric field through a thin passivation layer and avoiding their direct contact with the solution. The DEP force is achieved by insulating structures like iDEP, but avoids large heat buildup by applying the electric field only in the trapping region. The device consists of columns of offsetting microposts, which creates an arrangement where biological particles exposed to the smallest electric field gradient of the first column will subsequently be exposed to the location of the highest electric field gradient of the next column as the particles flow through the microchannel. Because of the micropost design, 100 % trapping can occur at lower voltages and thus lower electric field gradients, reducing both power consumption and negative side effects of electrothermal flow.

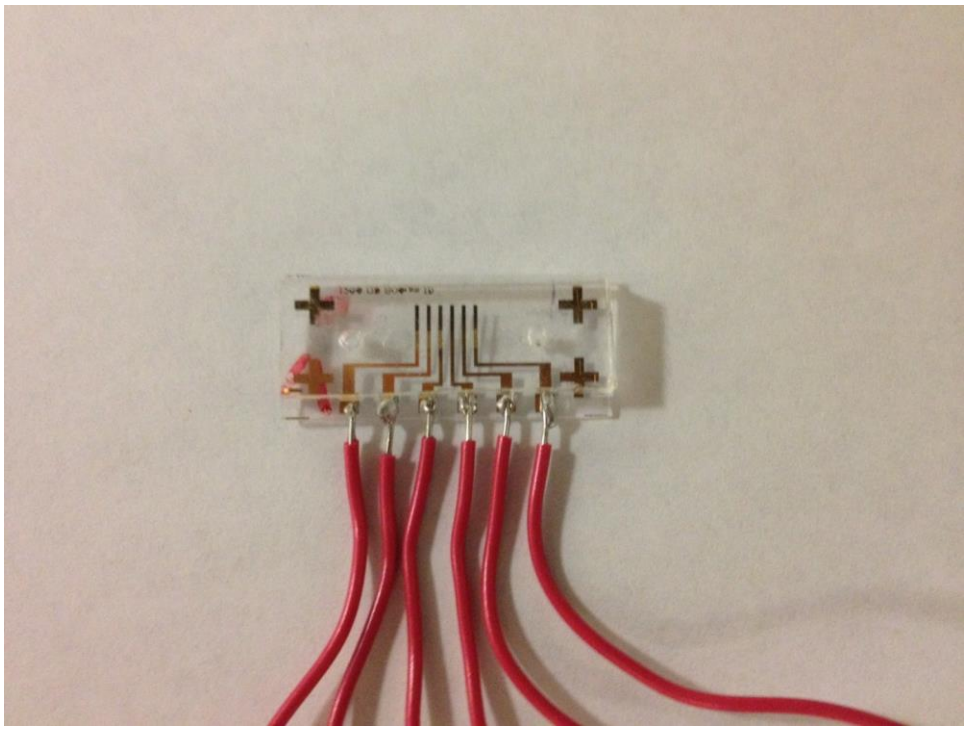

Figure 5 Photo of fabricated EπDEP device

This EπDEP device is comparable to the Virginia Tech MEMS Lab recently reported off-chip passivated-electrode insulator-based dielectrophoresis (OπDEP) devices [15], shown in Figure 6. A summary of these devices is included in the appendix. The EπDEP devices outperform the OπDEP devices by being able to achieve high capture efficiencies at both lower voltages and frequencies. This is due to the thin passivation layer of the EπDEP devices compared to the much thicker passivation layer required of OπDEP devices. This paper aims to demonstrate this technology by trapping both *Escherichia coli* (*E. coli*) and *Staphylococcus aureus* (*S. aureus*) cells within the microfluidic channel.

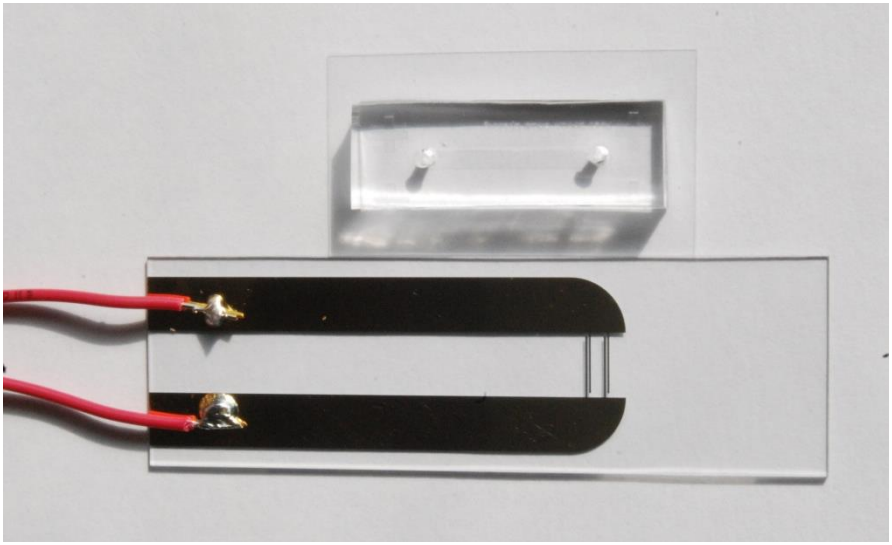

Figure 6 Photograph of OπDEP device.

2. Theory

The motion of polarizable particles suspended in dielectrically dissimilar media subjected to a spatially nonuniform electric field is dielectrophoresis [16]. Both dielectrophoresis and electrophoresis are based on Coulomb's law and the relationship of electric field intensity and charge. This is shown in equation 1.

$$\mathbf{F} = Q\mathbf{E} \qquad (1)$$

where **F** is the vector force, Q is the charge, and **E** is the electric field strength. Unlike electrophoresis, particles do not need to possess any net charge to be affected by DEP. If the particle is polarizable, meaning the charges within the particle can be attracted or repelled to the edges, creating a dipole, then the particle can be affected by a DEP force. Electrophoresis is illustrated in Figure 7.

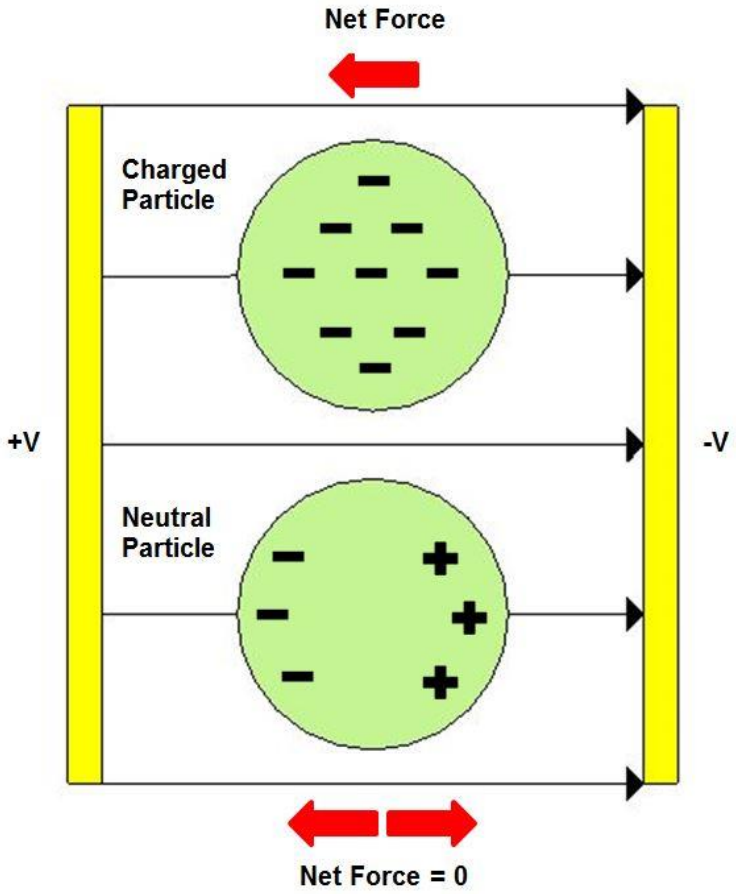

Figure 7 The Coulomb force on a charged particle is in either the direction or opposite direction of the electric field, which is electrophoresis. The Coulomb force on a neutral particle is net zero, therefore the particle is unaffected.

The charged particle has a net negative charge, thus it is attracted to the positive electrode and repelled by the negative one, based on equation 1. The neutral particle is polarizable, thus the charges will align with the electric field (negative charges on the edge of the particle closest to the positive electrode and positive charges on the edge closest to the negative electrode). However, the distribution of the positive charges directly mirrors the distribution of the negative charges, thus the net Coulomb force on the particle is zero.

Dielectrophoresis is illustrated in Figure 8 by the use of a nonuniform electric field. Similarly to the charged particle in Figure 7, the charges within the neutral particle will align

with the electric field. However, when the charges do align, they no longer mirror each other. The negative charges are more focused on the left edge of the particle compared to the positive charges on the right edge of the particle. Therefore, for this example, the vector sum of the Coulomb forces on the particle is not zero, illustrated by the different sized arrows within the figure. This nonzero Coulumb force on a neutral polarizable particle within a nonuniform electric field is dielectrophoresis.

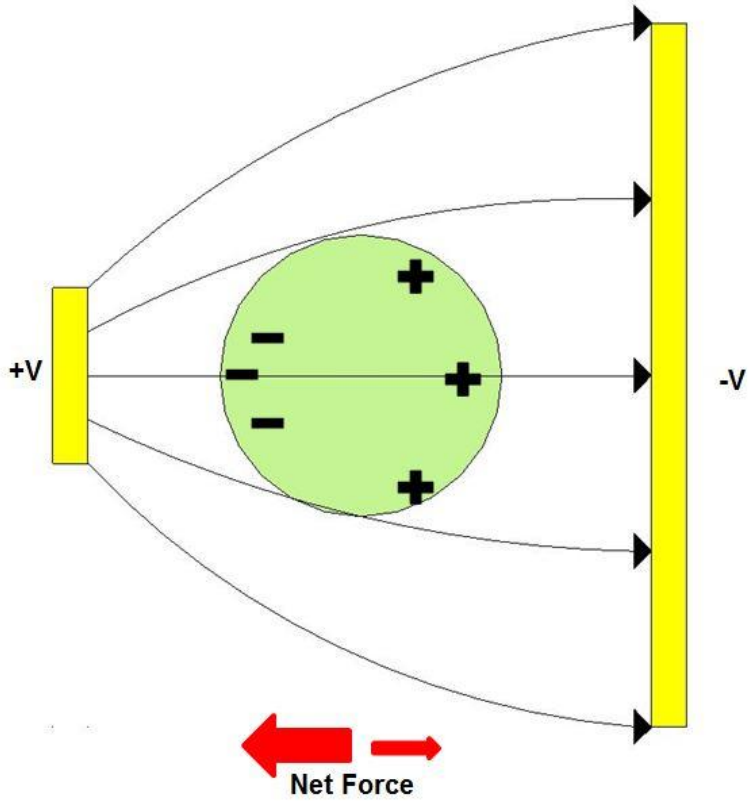

Figure 8 Schematic representation of dielectrophoresis

The DEP force on a spherical particle suspended in a medium is

$$\mathbf{F}_{\mathbf{DEP}} = 2\pi R^3 \varepsilon_m \,\mathrm{Re}[\, f_{CM}\,]\nabla(\mathbf{E}\bullet\mathbf{E}) \qquad (2)$$

where R is the radius of the particle, ε_m is the permittivity of the medium, and **E** is the local electric field. The previous equation can be derived for both homogenous and inhomogeneous spheres [17]. Re[f_{CM}] is the real part of the Clausius–Mossotti (CM) factor:

$$f_{CM} = (\varepsilon_p^{\,*} - \varepsilon_m^{\,*})/(\varepsilon_p^{\,*} + 2\varepsilon_m^{\,*}) \qquad (3)$$

where ε_p* and ε_m* are the complex permittivities of the particle and the medium, respectively. The complex permittivity is defined as follows:

$$\varepsilon^* = \varepsilon + \sigma/(j\omega) \qquad (4)$$

where ε is the real permittivity, σ is the real conductivity, and ω is the angular frequency of the applied potential signal. Because of the complex permittivity within the CM factor, $\mathbf{F}_{DEP}$ is a function of frequency and can be both positive and negative (opposing directions). If ε_p* is greater than ε_m*, then the CM factor is positive and the resulting DEP force is positive. However, if ε_p* is less than ε_m*, then the CM factor is negative, resulting in a negative DEP (nDEP) force. This concept is illustrated in Figure 9. The top particle in Figure 9 has a complex permittivity less than that of the medium and is therefore repelled from the region with the highest electric field gradient, demonstrating negative DEP. Conversely, the bottom particle has

a complex permittivity greater than that of the medium and is therefore attracted to the region with the highest electric field gradient, demonstrating positive DEP (pDEP).

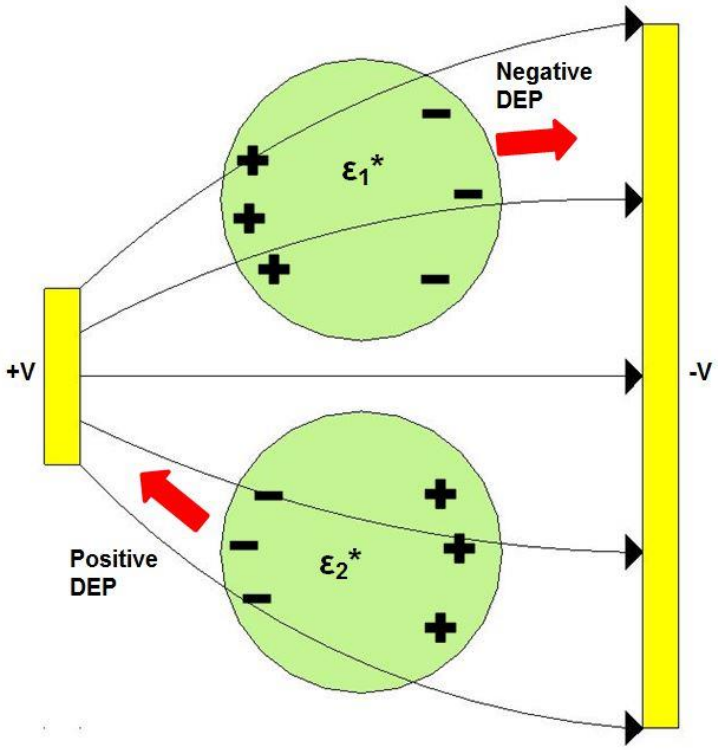

Figure 9 Schematic representation of dielectrophoresis of two polarized, neutral particles with different permittivities.

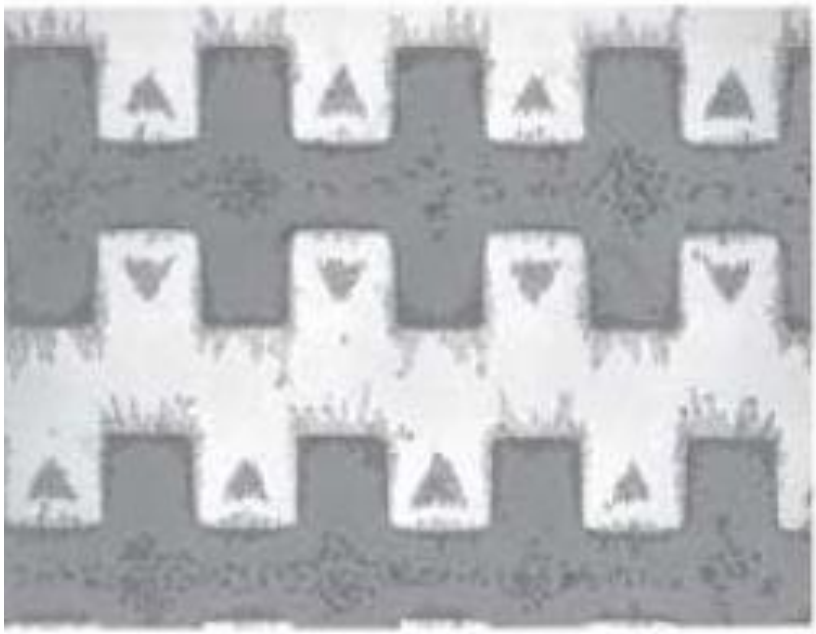

Figure 10 eDEP device demonstrating both pDEP and nDEP. Voldman, Joel. "Electrical Forces for Microscale Cell Manipulation." *Annual Review of Biomedical Engineering*. 2006. Used under fair use, 2014.

Figure 10 demonstrates both pDEP and nDEP simulataneously. The particles closest to the square-wave-like electrodes are experiencing pDEP, as they are being pulled to the electrodes. The particles bunched between the electrodes are experiencing nDEP, as they are being repelled by the electrodes. In order to achieve this difference, particles of different relative permittivities must be used, as demonstrated by Figure 9.

To understand the response of electric fields on biological particles, a shell model is used describing a cell as a sphere of highly conductive cytoplasm incased by a highly insulating membrane [19].

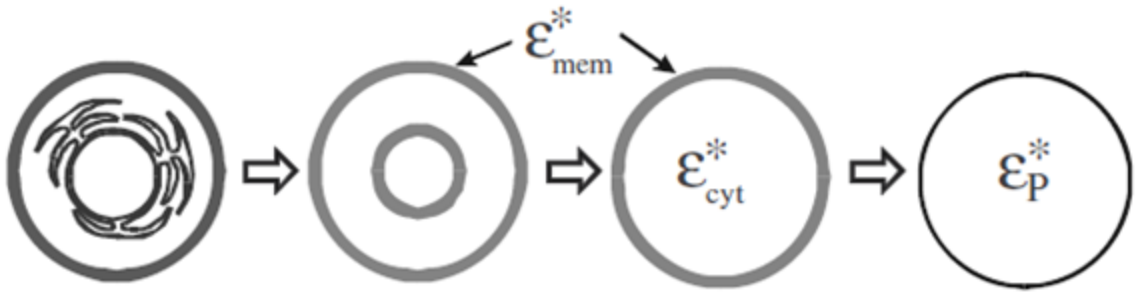

Figure 11 Schematic representation of the simplification of a biological cell into a sphere of relative permittivity. Pethig, Ronald. "Review Article – Dielectrophoresis: Status of the theory, technology, and applications." *Biomicrofluidics.* 2010. Used under fair use, 2014.

Figure 11 shows a schematic representation of the shell model. Each step shows a simplification of the cell, but the relative permittivities calculated from each step are kept to represent the cell. At low frequency and DC electric fields, the DEP force on bioparticles is determined by the size and conductivity. The resulting DEP force is then negative (nDEP) due to the CM factor. For high frequencies, the complex structure of the cell contributes more to the DEP response. Because of the relative permittivities of the cell wall and membrane, the CM factor will be positive, thus resulting in a positive DEP force (pDEP). The crossover frequency is the frequency point at which DEP force on a particle is zero as the DEP force passes from pDEP to nDEP or vice versa. This is demonstrated in Figure 12, which models the typical frequency response of a biological cell in a low conductivity electrolytic solution [20].

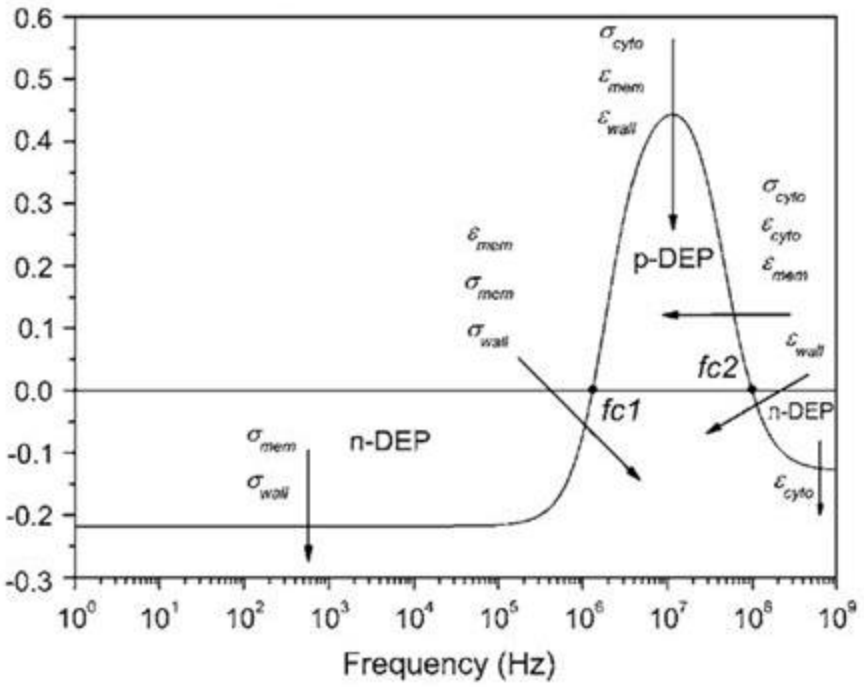

Figure 12 Model of typical frequency response of a biological cell in a low conductivity electrolytic solution. Castellarnau, M, A. Errachid, C. Madrid, A. Juarez, J. Samitier. "Dielectrophoresis as a Tool to Characterize and Differentiate Isogenic Mutants of Escherichia coli" *Biophysical Journal*. 2006. Used under fair use, 2014.

The fluid moving through the channel is pressure driven. The drag force on the bioparticles is approximated by

$$\mathbf{F}_{Drag} = 6\eta R\pi(u_{pf}) \qquad (5)$$

where R is the radius of the particle, η is the dynamic viscosity of the fluid, and u_{pf} is the relative velocity of the particle with respect to the fluid. For a particle to be trapped by the device, the DEP force must be higher in magnitude than the drag force. As shown by the equation, the drag force increases with fluid velocity, thus making DEP trapping more difficult at higher flow rates.

3. Methodology

3.1 Device design and fabrication

The microfluidic channel for the device has a cross section of 2 mm×50 μm and a length of 2 cm. The device uses a microfluidic channel with 200-μm polydimethylsiloxane (PDMS from Cole-Parmer) posts that are spaced 50 μm apart with 600 μm wide electrodes spaced 600 μm apart. The PDMS posts are 50 μm in height, ranging from the base to the ceiling of the microfluidic channel. Wider electrodes increase the capacitive coupling between the electrodes and the microfluidic channel, thus enabling DEP trapping at lower frequencies. In this device, the insulating structures create the nonuniform fields necessary for DEP. The device contains two columns of microposts centrally placed between the two electrodes.

The devices were fabricated in PDMS. A silicon wafer was patterned with photoresist (AZ9200, AZ Electronic Materials) and etched using an AMS-100 Deep Reactive Ion Etcher (Alcatel) to develop the structures. The photoresist was then stripped and the wafer was used as a master mold. The silicon wafer was anodically bonded to a glass wafer and then placed in a high temperature furnace so that the liquid glass conforms to the patterns etched in silicon. The silicon substrate was then etched away using KOH to obtain the glass mold for the microfluidic channel. The glass mold was cleaned and placed in a desiccator with a drop of trichloro(1,1,2,2-perfluoocytly) silane to form a monolayer on the surface of the mold, enabling easy peel-off. Liquid PDMS was mixed to a 10:1 ratio of PDMS monomer and curing agent and poured into the glass mold. After putting the setup into a vacuum chamber for 2 h to remove gas bubbles, it was cured for 45 min at 100 °C. Then, 2 mm holes were punched into the microchannels to form the fluidic ports. A 4-μm-thick passivation layer was created by pattering electrodes on a glass substrate followed by spinning and curing a thin layer of PDMS on top of this electrode

substrate. Then, the PDMS substrate containing the insulating structures was plasma-bonded directly to the electrode substrate. A fabrication process flow for the EπDEP devices is shown in Figure 13.

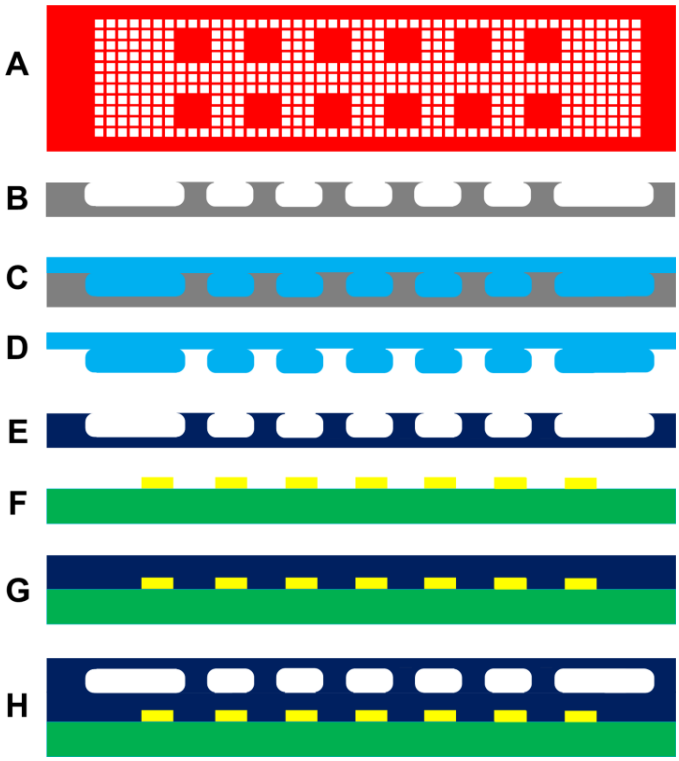

Figure 13 Fabrication process flow. (a) Photomask pattern (b) DRIE silicon etch (c) Glass reflow (d) KOH silicon etch (e) PDMS mold fabrication (f) Gold deposition (g) PDMS spinning (h) Plasma bonding

3.2 Analytical and numerical modeling

COMSOL Multiphysics 3.5 (COMSOL Inc., Burlington, MA) was used to determine the electric field distribution within the microchannel using numerical modeling. A 3D model was created for the device design and is shown in Figure 14. The electrical conductivities used for PDMS and deionized water were 8.20×10^{-13} and 3.00×10^{-4} S/m, respectively. The relative electrical permittivities used for PDMS and deionized water were 2.65 and 80, respectively. The

values for PDMS were provided by the manufacturer, while the permittivity of deionized water was assumed 80, and the electrical conductivity was measured using a conductivity meter (SG3-FK2, Mettler Toledo). The external boundaries of the device were set to electrical insulation except for the electrodes, which were given AC electric potentials. The simulation evaluated values of $\nabla |E|2$ as a function of position and frequency. The simulation predicts performance according to equation 2, which shows that for a given particle and medium, $\nabla |E|2$ is proportional to the DEP force on a particle.

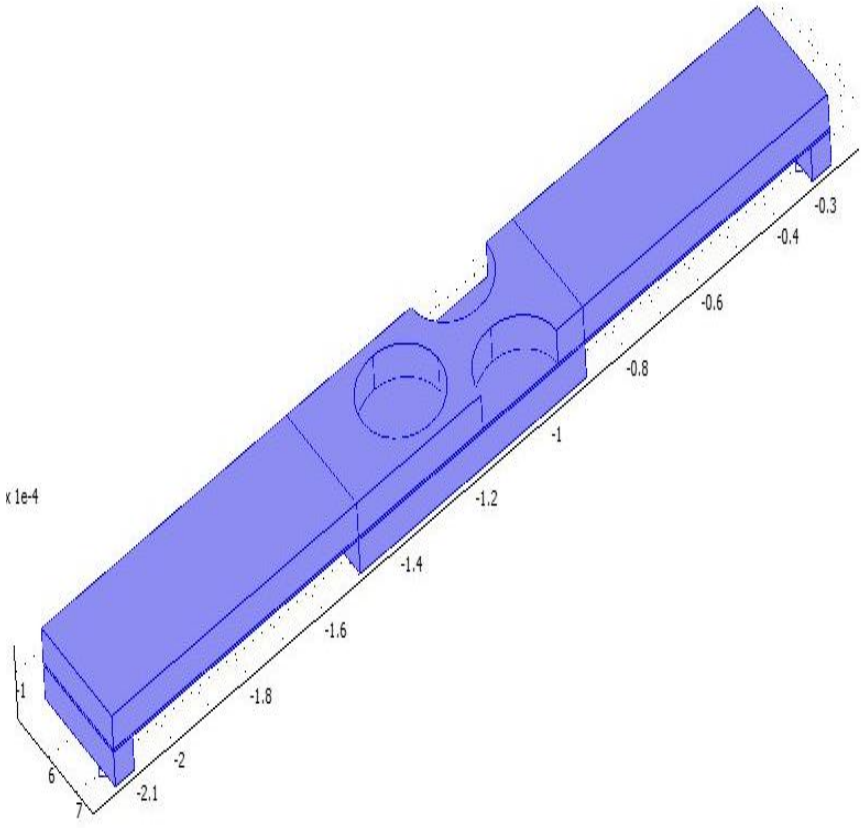

Figure 14 COMSOL simulation 3D geometry of the EπFRP device

3.3 Cell Preparation

E. coli strain MG1655 was grown at 37 °C in LB medium containing 1 % tryptone, 0.5 % NaCl, and 0.5 % yeast extract to a concentration of 4×10^8 cells/ml. Tetracycline was applied as antibiotic at a concentration of 5 μg/ml to enrich cells containing pHC60, a plasmid that carries a tetracycline resistance gene and constitutively expresses green fluorescence protein (GFP) which enables fluorescence microscopy analyses. *E. coli* cells for the experiments designated for live/dead cell separation did not contain pHC60. The cells for the live/dead experiments were stained by placing into live/dead solution (LIVE/DEAD BacLight, Invitrogen) for 20 min, according to manufacturer's protocol.

S. aureus strain ATCC 12600 was cultured in brain heart infusion media (BACTERIUS LIMITED, Houston, TX). The *S. aureus* cells were cultured in 100 ml at 37 °C and 165 rpm to the exponential growth phase (OD600~0.5). Cells were transferred into two sterile 50-ml centrifuge tubes and subjected to three washes by centrifugation (5,000×g for 10 min) followed by resuspension in 1× PBS. Bacteria were quantified microscopically using a hemocytometer (counting chamber) and by colony forming unit (CFU) counting of dilutions where colony numbers ranged between 30 and
300. To express a green fluorescence, the *S. aureus* cells were stained by placing into live solution (LIVE/DEAD BacLight, Invitrogen) for 20 min, according to manufacturer protocol.

For all experiments, the cells were centrifuged and resuspended three times in deionized (DI) water with a measured conductivity of 300 μS/m. The DI water conductivity was measured with a solution conductivity meter. The cells were diluted to a final concentration of 1×10^8 cells/ml prior to experimentation.

3.4 Experimental Setup

A function generator (4079, BK Precision) was connected to a power amplifier (A800DI, FLC) to produce an AC signal of 50 V peak-to-peak (Vpp) with frequencies from 1 kHz to 1 MHz. To ensure the accuracy of the waveform produced from the function generator, an oscilloscope (DL1300A, Yokogawa) was connected to monitor the output. Before conducting the experiments, the microfluidic devices were placed in a vacuum for at least one hour to reduce potential contaminants that would inhibit fluid flow through the device. During operation, the solution was pressure driven through the EπDEP device using a 1 mL syringe connected to a syringe pump (Pump 11 Elite, Harvard Apparatus). A waste reservoir was used to collect the solution that previously passed through the device. The DEP trapping was observed using an inverted fluorescent microscope (Axio Observer Z1), and videos and images of all experiments were captured using a CCD color camera (AxioCam Mrc). For experiments incorporating live/dead staining, a dual optical filter was used to differentiate between the bacteria.

With each DEP trapping data point, the flow rate of interest was applied for 15 seconds to ensure consistent flow rate through the channel. Then, the electric signal was applied and the subsequent DEP trapping recorded. The electric signal remained on for 30 seconds before switching off and releasing the trapped bacteria. After every video, the microchannels were inspected for bacteria fouling between the microposts; when necessary, any fouled bacteria were removed by increasing the flow rate of the syringe pump briefly. This ensured that each data point included only bacteria trapped during that particular experiment run.

To quantify the trapping effectiveness of the chip, a light intensity measurement was used. The *E. coli* cells express GFP which acted as a fluorescent stain. The *S. aureus* cells were fluorescently stained prior to the DEP trapping experiments. During the DEP trapping

experiments, as the number of trapped cells increased, the intensity of the light also increased. To analyze the DEP trapping videos, ImageJ (NIH) was used. In ImageJ, a region of interest was selected around the microposts where the DEP trapping occurred, and the intensity of the light was quantized for the last frame before the electric signal was removed. The region of interest was held constant throughout the experiments. The results of 10 experiments were averaged at each applied signal frequency.

The metric used to quantify the trapping effectiveness of the device is the capture efficiency defined as follows:

$$CE=[(I-O)/I] \times 100\% \qquad (6)$$

where I is the number of incoming bacteria observed in a single frame of a DEP trapping video, and O is the number of escaped bacteria observed in a single frame of a DEP trapping video. The measurements were made by counting the bacteria upstream (I) and downstream (O) of the trapping region in the individual frames of the videos taken during the experiments. To acquire this data, high speed video software (Zen, Zeiss) was used to produce high resolution frames to enable enumeration of the bacteria. The regions used for counting the upstream and downstream bacteria were identically sized rectangles and remained constant throughout the experiments. Ten fluid flow velocity sweeps from 100 µL/hr to 2000 µL/hr were completed. To obtain a data point representing one flow rate, the respective values of I and O were averaged over the ten flow sweeps. For cases where the bacterial cells remained in clusters after being released, the clusters were assumed to be flat, and their respective size was used to estimate the number of

cells in the cluster. It should be noted that if the clusters had multiple cells stacked in depth, this method would underestimate the number of bacteria.

4. Results

4.1 Numerical Modeling

The results from the numerical model are displayed in the figures below. In Figure 15, the $\nabla(E \bullet E)$ slice plot with an applied electrical signal of 50 Vpp at 300 kHz is shown. The highest field gradients were observed at the locations near to the insulating structures, a characteristic typical of iDEP devices [21]. The peak gradient was determined to be 4.2×10^{14} $[(m \bullet kg^2)/(s^6 \bullet A^2)]$. Based on Equation 2, $\nabla(E \bullet E)$ is proportional to the DEP force on a particle. In previously reported iDEP devices, DC voltages of 800 V were required to obtain optimum DEP forces [22]. By embedding the electrodes and capacitively coupling through a thin passivation layer, high electric field gradients can be achieved at low AC voltages.

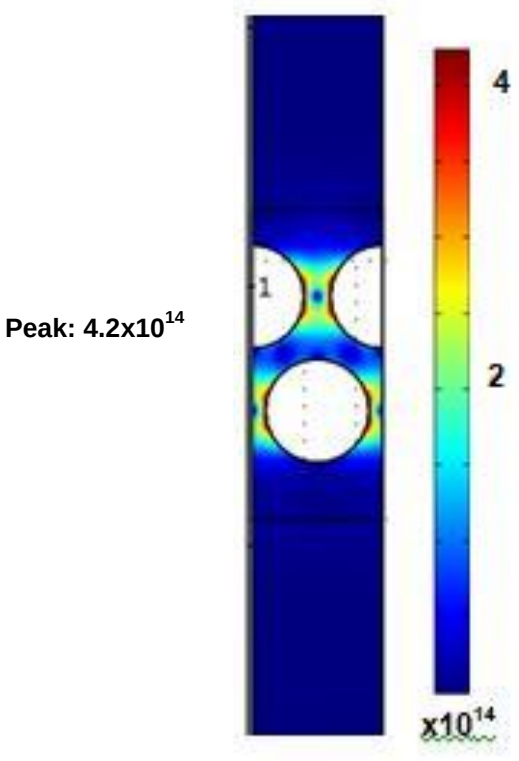

Figure 15 COMSOL simulation slice plot of $\nabla(E \cdot E)$ at 300 kHz and 50 Vpp

Figure 16 shows the frequency response of the EπDEP devices at applied AC voltages of 50 V_{pp} and 400 V_{pp}. As shown in the figure, the electric field gradient remains high at very low frequencies; this creates a wide range suitable for DEP trapping. Previously reported OπDEP devices were able to achieve a peak electric field gradient of 2.27×10^{15} $[(m \bullet kg^2)/(s^6 \bullet A^2)]$ at an applied voltage of 400 $Vpp_{[15]}$. For comparison, the EπDEP device was able to achieve a peak electric field gradient of 2.52×10^{16} $[(m \bullet kg^2)/(s^6 \bullet A^2)]$ at 400 Vpp. Therefore, the EπDEP devices can achieve comparable electric field gradients within the channel at lower applied voltages.

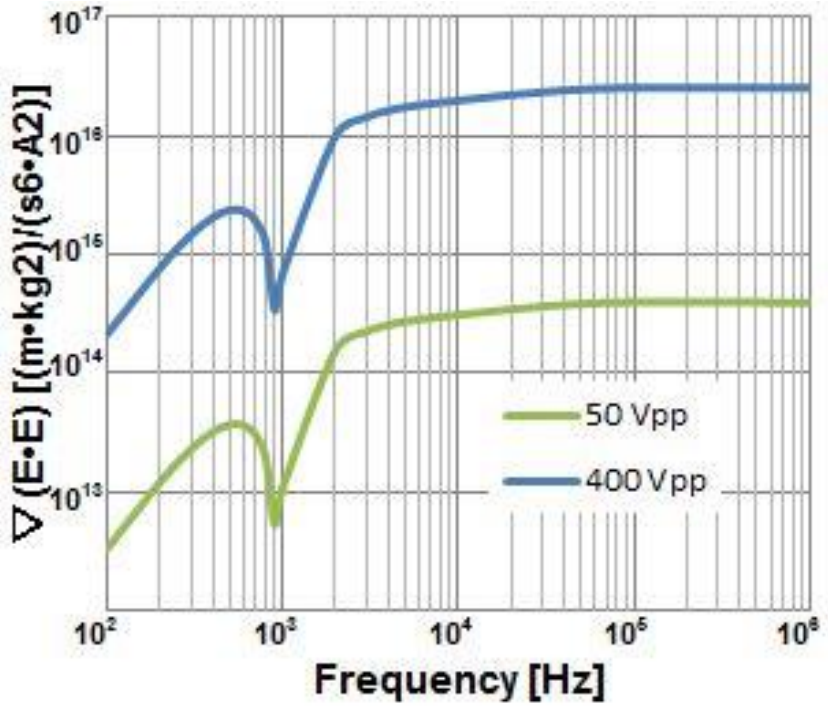

Figure 16 Maximum simulation values of ▽(E•E) as a function of frequency.

To demonstrate the effectiveness of reducing the passivation layer between the electrodes and channel, a series of simulations were performed evaluating $\nabla(E \bullet E)$ as a function of passivation layer thickness. Simulations were performed using thicknesses of 5, 10, 20, 40, 60, and 100 µm. The results of these simulations are shown in Figure 17. The simulation clearly demonstrates that as the passivation layer is decreased, the effective DEP force increases due to an increase in $\nabla(E \bullet E)$.

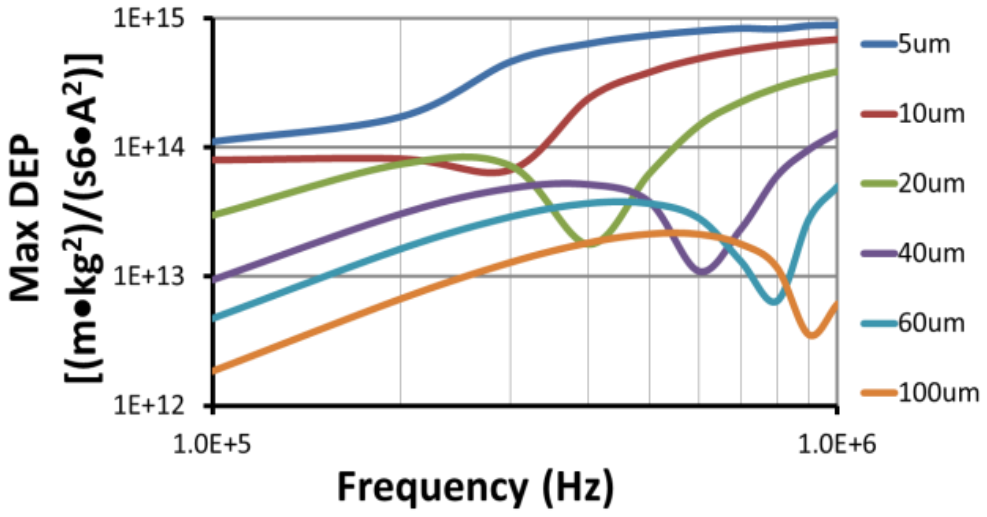

Figure 17 The effect of different passivation layer thicknesses on the DEP force.

4.2 Frequency Response

Bacteria trapping experiments were performed with the applied electric signal of 50 Vpp. The device was able to obtain 100% capture efficiency of bacteria with the applied pressure-driven flow. The experimental performance of the EπDEP devices at different applied frequencies and a fixed flow rate of 100 µl/hr are shown in Figure 18, which is a plot of light intensity within the DEP trapping region as a function of frequency for *E. coli*. Because *S.*

aureus responded very similarly to *E. coli*, the data is not shown. It has been previously reported that *E. coli* and *S. aureus* differ in trapping intensity as a function of frequency, but in this study differences were only observed at frequencies greater than 1 Mhz [23]. Due to the power amplifier limitation, it should be noted that the amplitude of the amplified signal began to attenuate at 400 kHz, which led to a decrease in DEP trapping at higher frequencies.

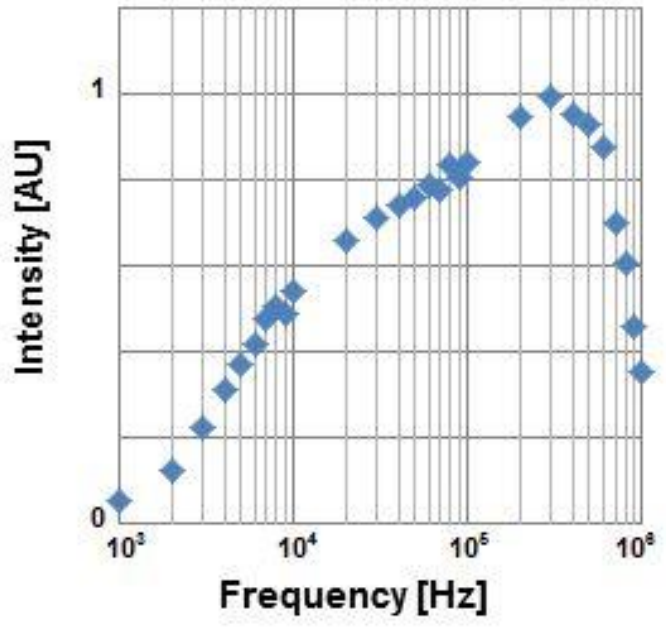

Figure 18 Experimentally observed DEP trapping of *E. coli* and *S. aureus* in EπDEP for an applied electrical signal of 50 Vpp and flow rate of 100 µL/hr. Graph show quantized light intensity in the trapping region as a function of frequency

Figure 19(a) and (b) show the variability of trapping strength as a function of frequency for *E. coli*. Figure 19(c) and (d) show the variability of trapping strength as a function of frequency for *S. aureus.* Maximum trapping occurred at 200 – 300 kHz, in which no bacteria were observed escaping the trapping region, thus the CE was 100%. The results match the predicted performance from the numerical models. From the model, the strongest DEP force occurred in the regions closest to the microposts. As the distance from the microposts increased, the strength of the DEP force decreased. Thus, the area centrally located between the microposts exhibited

the weakest DEP force. If the DEP force is not strong enough, bacteria traveling along the centerline will not be trapped. As previously reported in OπDEP devices, the electric field gradient must be at least 1×10^{15} to achieve 100% trapping efficiency [15]. However, because the EπDEP device is designed with offsetting columns of microposts, bacteria migrating along the centerline of the first column of microposts will not be trapped within the first trapping region, but instead be trapped within the second column of microposts. As a result of device design, high trapping efficiency occurred with lower electric field gradients. This creates an additional advantage of reduced electrothermal fluid flow, which is proportional to the electric field gradient [24].

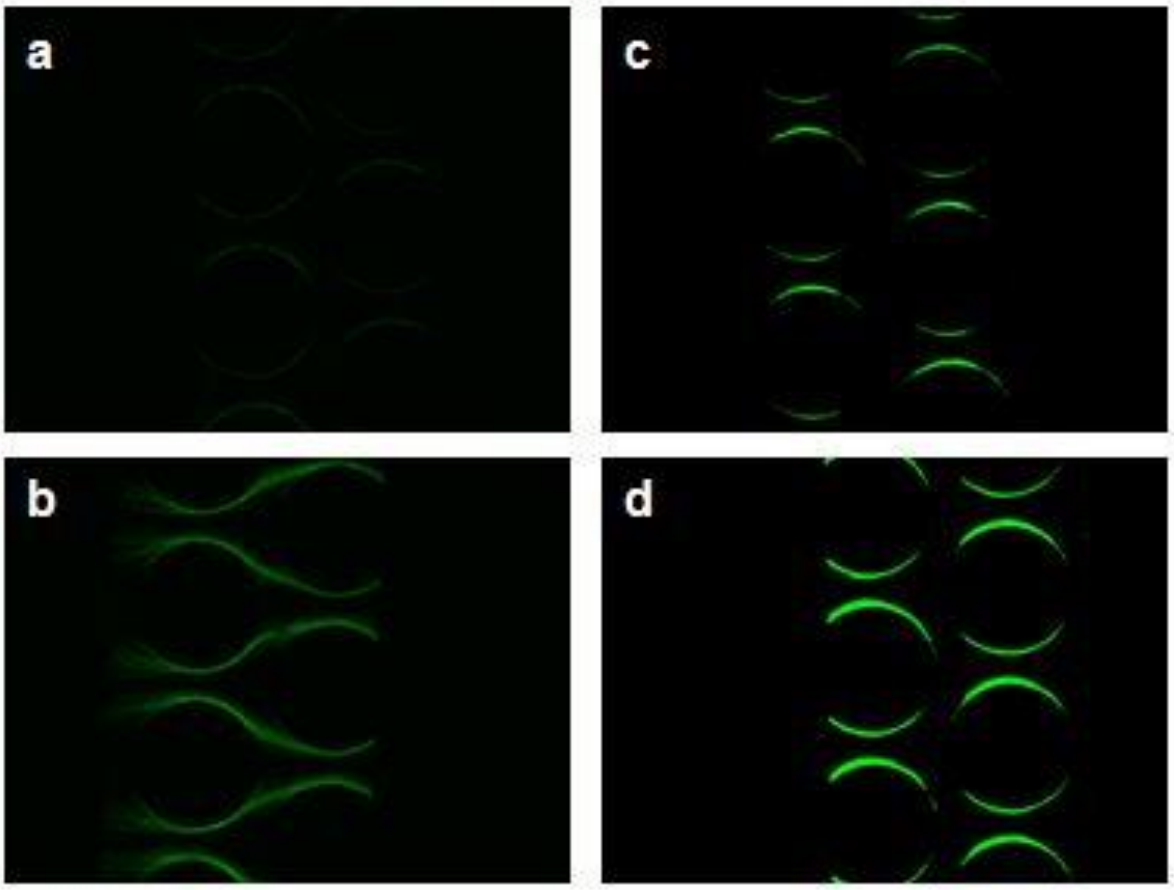

Figure 19 (a) *E. coli* at 10 kHz (b) *E. coli* at 300 kHz (c) *S. aureus* at 10 kHz (d) *S. aureus* at 300 kHz

4.3 Flow Rate

Because the highest trapping efficiency occurred at 300 kHz, the applied electrical signal was kept constant at 50 V_{pp} at a frequency of 300 kHz for the fluid flow velocity sweeps. Figure 20 shows the capture efficiency as a function of flow rate. Figure 21(a) and Figure 21(b) show the variability of *E. coli* trapping as flow rate changed. The devices were able to consistently achieve a CE of 100% up to flow rates of 500 µl/hr. As the flow rate increased beyond 500 µl/hr, CE slowly decreased linearly. DEP trapping still occurred with 50% efficiency at 2,000 µl/hr. This outperforms our previously reported OπDEP device, which was able to achieve a CE of 100% at flow rates up to 400 µL/hr, and achieved a CE up to 50% CE at 1300 µL/hr [15]. Our current results show a maximum throughput with 100% CE at 500 µl/hr. In addition, the EπDEP devices can be operated at flow rates of 2,000 µl/hr if only preconcentration is desired without the need for high capture efficiencies.

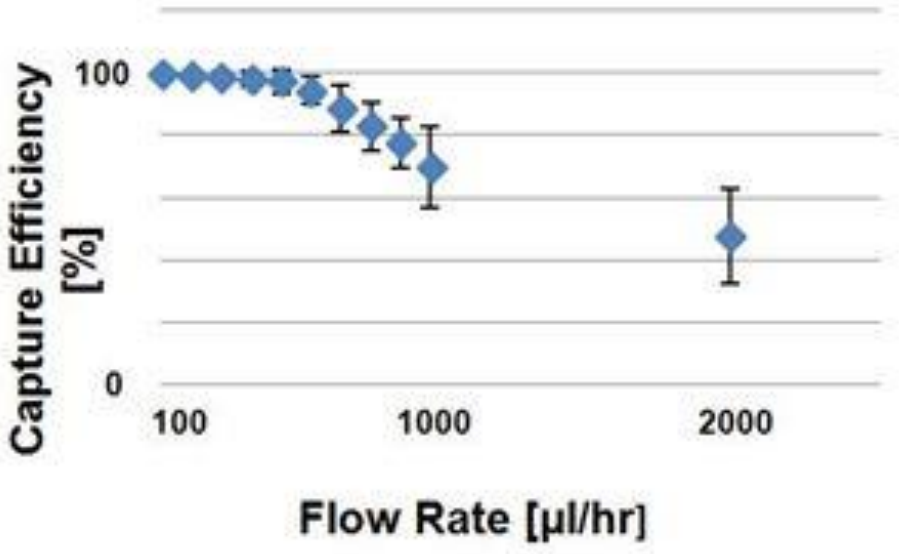

Figure 20 Capture efficiency as a function of flow rate. Error bars shown for 1 standard deviation

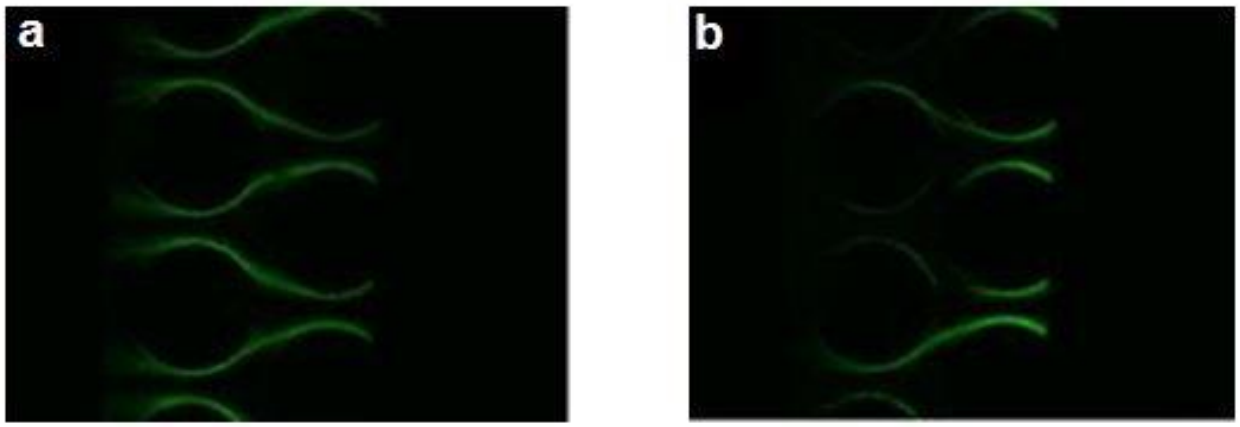

Figure 21 Observed DEP trapping of *E. coli* in EπDEP device at an applied electrical signal of 50 Vpp at 300kHz with pressure driven flow at (a) 100 µL/hr (b) 700 µL/hr

4.4 Separation of Particles

To demonstrate the EπDEP ability to selectively concentrate different types of biological samples, a solution containing both live and dead E. coli cells was stained with live/dead solution. Figure 22 demonstrates that the live bacteria were trapped and released on the microposts while the dead bacteria were not. It should be noted that some of the dead cells did foul to the surface of the chip before any electric signal was applied as shown in Figure 22(a). Based on observation, the frames immediately after removing an electric signal show only green fluorescence cells being released as displayed in Figure 22(c).

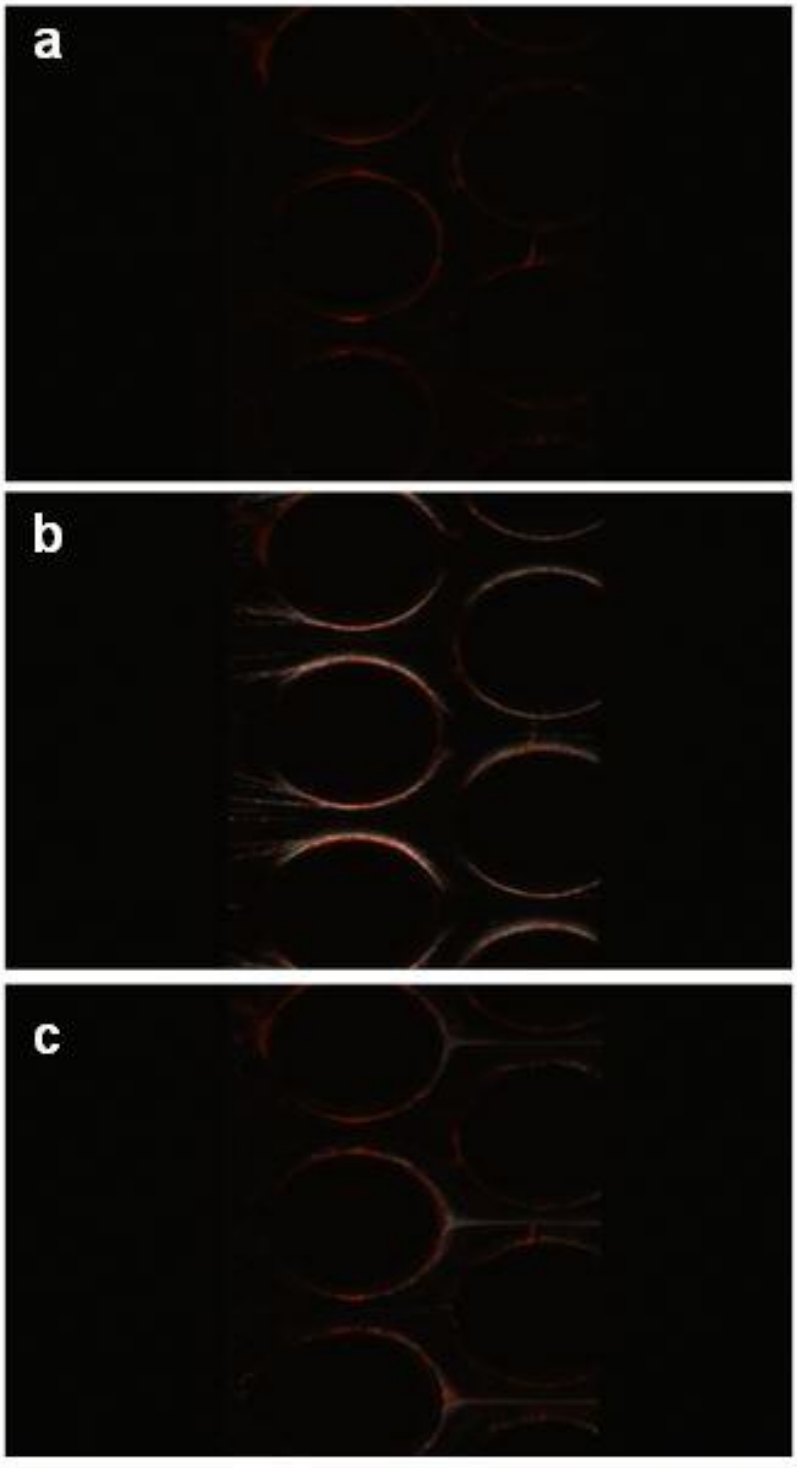

Figure 22 Selective trapping of live *E. coli* (white) from dead *E. coli* (red) (a) No applied voltage (b) 50 Vpp at 300 kHz is applied for 30 seconds (c) Voltage is turned off and the live bacteria are released

5. Conclusion

5.1 Discussion

This work has introduced a new technique capable of achieving high efficiency trapping of bioparticles at low voltages and demonstrated the device through modeling and experiments. EπDEP draws from advantages of both iDEP and eDEP principles, while avoiding common shortcomings of these methods. The disadvantage of Joule heating typical of iDEP devices is removed, which is evident by the lack of electroosmotic flow [13], due to two factors implemented in these devices. The applied electric signal is much smaller than typical iDEP devices, leading to less current within the microfluidic channel. Also, decreased electrode spacing allows only a small part of the microfluidic channel to have current running through it, leading to less material to cause resistive heating. The heat buildup can cause device failure [25] as well as reduce sample viability rate in biological applications [18]. Therefore, EπDEP devices can operate for longer periods of time with minimized temperature effects on the biological particles. Electrode deterioration typical of eDEP devices is also avoided due to the fact that EπDEP utilizes contactless embedded electrodes that operate by capacitive coupling within the microfluidic channel. This is also advantageous by avoiding direct electrode contact with the solution, which could lead to cell contamination and gas evolution. A summary of the advantages and disadvantages of eDEP, iDEP, OπDEP, and EπDEP are shown in Table 1.

	eDEP	iDEP	OπDEP	EπDEP
Advantages	- Flexibility in electrode shape design	- Flexibility in insulating structure design - Easy to mass produce	- Chip is disposable and easy to mass produce - No electrode contact with solution - No heat buildup near insulating structures - Flexibility in electrode shape design - Flexibility in insulating structure design	- Chip operates at very low voltages with high efficiency - No electrode contact with solution - No heat buildup near insulating structures - Flexibility in electrode shape design - Flexibility in insulating structure design
Disadvantages	- Decline in performance as more particles are concentrated - Electrodes must contact the solution - Chip must be cleaned before reuse	- Large heat buildup near insulating structures - Electrodes must contact solution - Requires large DC voltages to operate	- Require larger applied AC voltages to achieve high particle capture efficiency	- More time-consuming to fabricate embedded electrodes - Chip must be cleaned before reuse

Table 1 Summary of advantages and disadvantages of eDEP, iDEP, OπDEP, and EπDEP chip designs.

The thin passivation layer was created by spinning a layer of PDMS onto the electrode substrate, thus the thickness can be chosen arbitrarily. By adjusting the thickness of the passivation layer, one can adjust the device for various applications of different applied electrical signals. Because the device operates at low voltages, less complex electronics can be used during application. High voltages could lead to problems such as cell death due to electroporation. To avoid this, previous attempts required the electric signal to only be applied in short bursts [26]. EπDEP can continuously operate at low voltages without risking cell death. The channel design of large, offsetting columns of microposts increases efficiency leading to a CE of 100% at flow

rates of 500 μL/hr and an applied voltage of 50 V_{pp}. Because of the large microposts capable of supporting large channels the throughput of the device is scalable. Because the electrodes generating the electric field are implemented across the channel width and the DEP forces are created by insulting posts, the microchannel can be widened as far as fabrication allows. By widening the microchannel, a higher throughput of fluid can be achieved. To characterize various biological particles, signal parameters such as signal magnitude and frequency can be adjusted in real time, creating easily manipulated independent variables. By applying multiple trapping zones in series, various methods of multiple particle characterization and separation can be achieved in a single device operation. The devices have also been shown to successfully separate live bacteria cells from dead cells. This is significant because DNA-based assays, which are currently the most precise in specificity, cannot readily distinguish between live and dead cells. Available means of viability testing, including culturing or staining bacteria and microscopy imaging [27], are labor intensive and still do not guarantee discrimination against all dead cells (microscopy) or capture all live cells (culturing).

5.2 Future Work

The EπDEP devices can be customized to meet a wide variety of applications. DEP deflection based devices [28,29] used to deflect particles in particular channels can be used by applying very low voltages and weakening respective DEP force. Also, 3D constrictions [30,31], which utilizes insulating structures designed to constrict the channel in both the horizontal and vertical directions can be developed. In future work, the following aspects should be considered:

- Exploration of EπDEP devices with 3D structures to improved DEP forces, thus creating devices capable of achieving high trapping efficiencies at much higher flower rates.
- Creating full systems on a chip. This would include the detection mentioned in this work, but would also include filtering, separating, and electrically sensing various pathogens. An example of a separate system than demonstrated by the EπDEP devices in shown in Figure 23
- Explore the use of EπDEP devices for more applications including proteins, fungi, mammalian cells, etc. An example of EπDEP devices designed for applications with mammalian cells is shown in *A. EπDEP and Mammary* Cancer Cells with the Appendix
- Customize the devices to create independent profiles for various types of pathogens

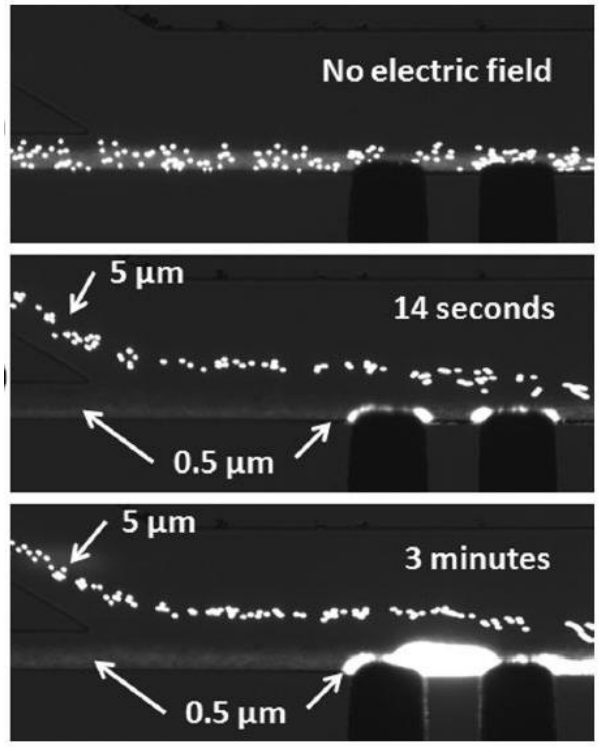

Figure 23 Demonstration of separating particles. Lewpiriyawong, N. C. Yang. "AC-dielectrophoretic characterization and separation of submicron and micron particles using sidewall AgPDMS electrodes." *Biomicrofluidics*. 2012. Used under fair use, 2014.

References

1. Corvalan P (2006) Preventing disease through healthy environments. World Health Organization

2. Pruss-Ustun A (2008) Safer Water, Better Health. World Health Organization

3. Kua C, Y.C. Lam, C. Yang, and K. Youcef-Toumi (2005) Review of bio-particle manipulation using dielectrophoresis.

4. Zhang C, Khoshmanesh K, Mitchell A, Kalantar-zadeh K (2010) Dielectrophoresis for manipulation of micro/nano particles in microfluidic systems. Anal Bioanal Chem 396 (1):401-420. doi:10.1007/s00216-009-2922-6

5. Çetin B, Li D (2011) Dielectrophoresis in microfluidics technology. ELECTROPHORESIS 32 (18):2410-2427. doi:10.1002/elps.201100167

6. Zhou R, Wang P, Chang H-C (2006) Bacteria capture, concentration and detection by alternating current dielectrophoresis and self-assembly of dispersed single-wall carbon nanotubes. ELECTROPHORESIS 27 (7):1376-1385. doi:10.1002/elps.200500329

7. Nakano A, Ros A (2013) Protein dielectrophoresis: Advances, challenges, and applications. ELECTROPHORESIS 34 (7):1085-1096. doi:10.1002/elps.201200482

8. Grom F, Kentsch J, Müller T, Schnelle T, Stelzle M (2006) Accumulation and trapping of hepatitis A virus particles by electrohydrodynamic flow and dielectrophoresis. ELECTROPHORESIS 27 (7):1386-1393. doi:10.1002/elps.200500416

9. Kang Y, Cetin B, Wu Z, Li D (2009) Continuous particle separation with localized AC-dielectrophoresis using embedded electrodes and an insulating hurdle. Electrochimica Acta 54 (6):1715-1720. doi:http://dx.doi.org/10.1016/j.electacta.2008.09.062

10. Golan S, Elata D, Orenstein M, Dinnar U (2006) Floating electrode dielectrophoresis. ELECTROPHORESIS 27 (24):4919-4926. doi:10.1002/elps.200600208

11. Huang Y, Pethig R (1991) Electrode design for negative dielectrophoresis. Measurement Science and Technology 2 (12):1142-1146. doi:10.1088/0957-0233/2/12/005

12. Green NG, Morgan H (1997) Dielectrophoretic separation of nano-particles. Journal of Physics D: Applied Physics 30 (11):L41-L44. doi:10.1088/0022-3727/30/11/001

13. Sridharan S, Zhu J, Hu G, Xuan X (2011) Joule heating effects on electroosmotic flow in insulator-based dielectrophoresis. Electrophoresis 32 (17):2274-2281. doi:10.1002/elps.201100011

14. Srivastava SK, Gencoglu A, Minerick AR (2011) DC insulator dielectrophoretic applications in microdevice technology: a review. Anal Bioanal Chem 399 (2):301

15. Zellner P, Agah M (2013 (In Press)) Off-Chip Passivated-Electrode, Insulator-Based Dielectrophoresis. Anal Bioanal Chem

16. Pohl HA (1951) The Motion and Precipitation of Suspensoids in Divergent Electric Fields. Journal of Applied Physics 22 (7):869-871. doi:10.1063/1.1700065

17. Pethig R (2010) Review Article---Dielectrophoresis: Status of the theory, technology, and applications. Biomicrofluidics 4 (2):022811-022835

18. Voldman J (2006) Electrical forces for microscale cell manipulation. Annual review of biomedical engineering 8 (1):425-454. doi:10.1146/annurev.bioeng.8.061505.095739

19. Polk C, Postow E (1996) Handbook of biological effects of electromagnetic fields. vol Book, Whole. CRC Press, Boca Raton, FL

20. Castellarnau M, A. Errachid, C. Madrid, A. Juarez, and J. Samitier (2006) Dielectrophoresis as a Tool to Characterize and Differentiate Isogenic Mutants of Escherichia coli. Biophysical Journal 91 (10):3927-3945

21. Zellner P, Agah M (2012) Silicon insulator-based dielectrophoresis devices for minimized heating effects. Electrophoresis 33 (16):2498-2507. doi:10.1002/elps.201100661

22. Martínez-López J, Moncada-Hernández H, Baylon-Cardiel J, Martínez-Chapa S, Rito-Palomares M, Lapizco-Encinas B (2009) Characterization of electrokinetic mobility of microparticles in order to improve dielectrophoretic concentration. Anal Bioanal Chem 394 (1):293-302. doi:10.1007/s00216-009-2626-y

23. Sanchis A, Brown AP, Sancho M, Martínez G, Sebastián JL, Muñoz S, Miranda JM (2007) Dielectric characterization of bacterial cells using dielectrophoresis. Bioelectromagnetics 28 (5):393-401. doi:10.1002/bem.20317

24. Green NG, Ramos A, González A, Castellanos A, Morgan H (2001) Electrothermally induced fluid flow on microelectrodes. Journal of Electrostatics 53 (2):71-87. doi:10.1016/S0304-3886(01)00132-2

25. Sabounchi P, Huber DE, Kanouff MP, Harris AE, Simmons BA Joule heating effects on insulator based dielectrophoresis. In: 12th Int Conf on Miniaturized Systems for Chemistry and Life Sciences, San Diego, CA, USA, 2008. pp 12-16

26. Dower WJ, Miller JF, Ragsdale CW (1988) High efficiency transformation of E. coli by high voltage electroporation. Nucleic acids research 16 (13):6127-6145. doi:10.1093/nar/16.13.6127

27. Jones KH, Senft JA (1985) An improved method to determine cell viability by simultaneous staining with fluorescein diacetate-propidium iodide. The journal of histochemistry and cytochemistry : official journal of the Histochemistry Society 33 (1):77-79. doi:10.1177/33.1.2578146

28. Daugherty PS, Heeger AJ (2005) Marker-Specific Sorting of Rare Cells Using Dielectrophoresis. Proceedings of the National Academy of Sciences of the United States of America 102 (44):15757-15761. doi:10.1073/pnas.0507719102

29. Hawkins BG, Smith AE, Syed YA, Kirby BJ (2007) Continuous-flow particle separation by 3D Insulative dielectrophoresis using coherently shaped, dc-biased, ac electric fields. Analytical chemistry 79 (19):7291-7300. doi:10.1021/ac0707277

30. Chu H, Doh I, Cho YH (2009) A three-dimensional (3D) particle focusing channel using the positive dielectrophoresis (pDEP) guided by a dielectric structure between two planar electrodes. LAB ON A CHIP 9 (5):686-691. doi:10.1039/b812213j

31. Zellner P, Renaghan L, Hasnain Z, Agah M (2010) A fabrication technology for three-dimensional micro total analysis systems. Journal of Micromechanics and Microengineering 20 (4):045013-045013. doi:10.1088/0960-1317/20/4/045013

32. Lewpiriyawong, N, C. Wang. AC-dielectrophoretic characterization and separation of submicron and micron particles using sidewall AgPDMS electrodes (2012). Biomicrofluidics 6 (1):012807-012807-012809. doi:10.1063/1.3682049

Appendix

A. EπDEP and Mammary Cancer Cells

Experimentation was successfully performed in trapping and manipulating mammary cancer cells (MDA-MB-468) with similar concept devices. The EπDEP devices used were different than the previous devices only in channel designs. Because of the relative size difference between (MDA-MB-468 cells are 5 to 10 times larger than bacteria cells), the channel was designed differently. Also, because MDA-MB-468 cells are less durable, the channels were designed with smaller and less insulating posts to weaken the DEP forces within the microchannel. A schematic of the EπDEP devices are shown in Figure 24.

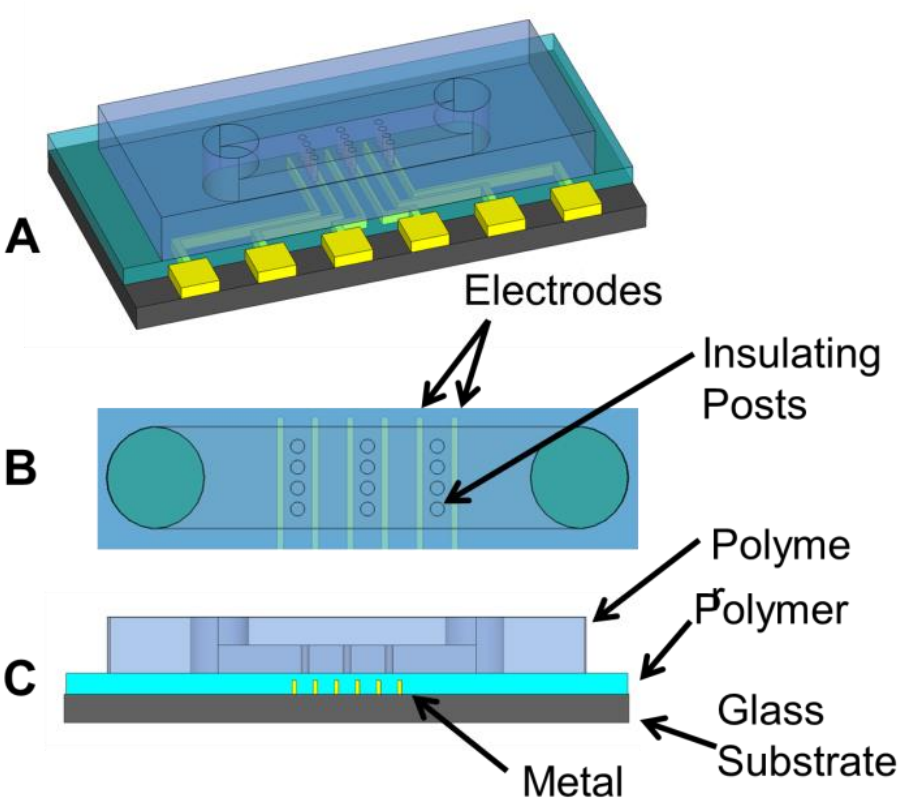

Figure 24 Schematic of EπDEP devices used in MDA-MB-468 experiments

The devices were design with a single vertical column of insulated microposts (100 µm diameter, 50 µm spacing) located between electrodes (400 µm wide, 600 µm horizontal spacing) to generate the non-uniform electric field lines to concentrate the mammalian cells while maintain stead flow within the channel. The fabrication of these devices was identical to the process described in Chapter 3.1.

MDA-MB-468 cells were harvested from a confluent T-75 flask by trypsinization. The cells were suspended in 1mL cell culture medium (DMEM, 10%FBS, 1%Penicillin-Streptomycin, 1% L-glutamine) and centrifuged at 1000rpm for 6 min. The cell culture medium was removed and the cells were suspended in 1mL of DEP buffer (8.5g sucrose and 0.725mL RPMI in 100mL DI water) for experiments. The cells were fluorescently stained green with Calcein AM (BD Biosciences) to visualize them during experiments.

The results are shown in Figure 25. The capture efficiency was quantified by counting the cells in time-lapse images and calculated as the ratio of the number of incoming cells due to flow. As can be seen in Figure 25, more than 90% trapping was obtained for frequencies in the range of 400 kHz – 1MHz. The maximum trapping of 97% was observed at 500 kHz. Figure 26 shows screenshots of the captured cells at 300 kHz, 500 kHz, and 1 MHz, respectively. These results demonstrate that EπDEP technology can be used to manipulate mammalian cells and inspires interest in further studies to evaluate the sensitivity of the EπDEP devices.

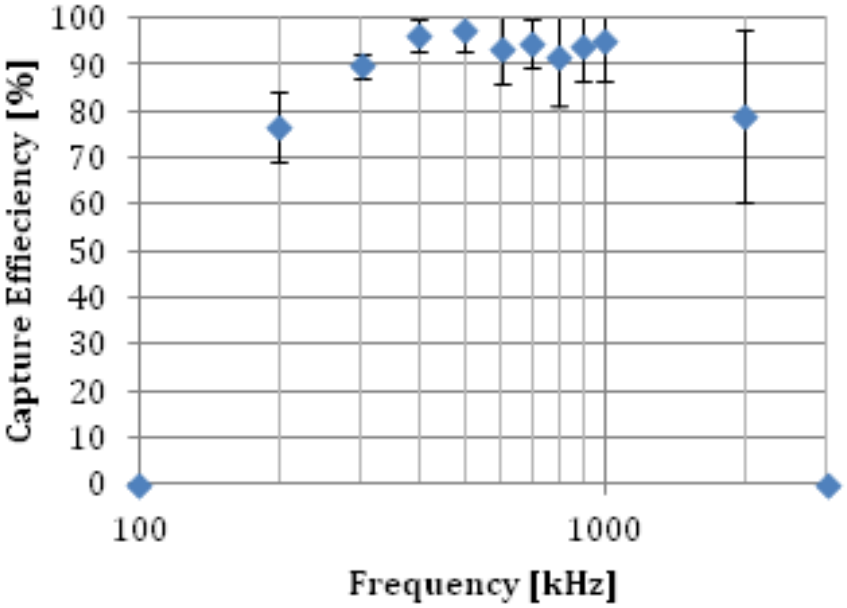

Figure 25 Observed DEP trapping efficiency of MDA-MB-468 as a function of frequency.

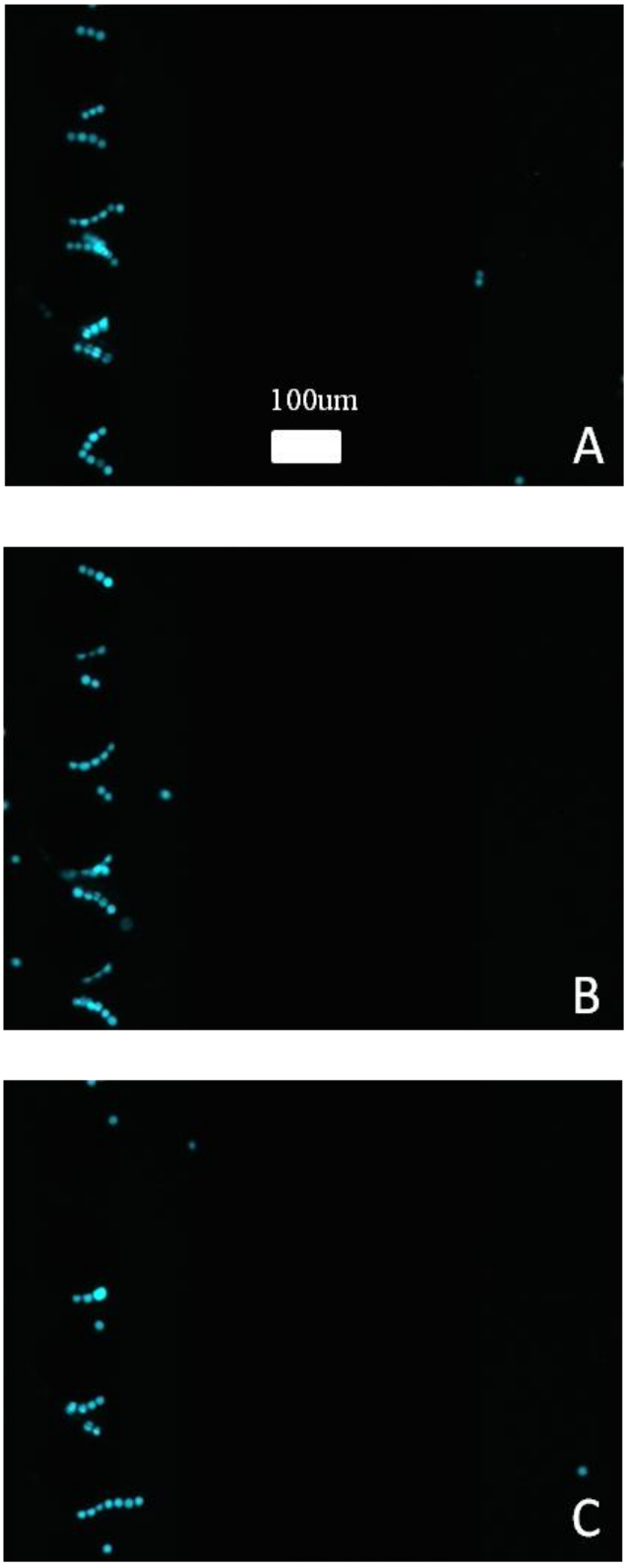

Figure 26 DEP trapping of MDA-MB-468 cells with 300 Vpp at (a) 300kHz (b) 500kHz (c) 1MHz

B. OπDEP

OπDEP devices were mentioned in comparison to the EπDEP devices. These devices were designed to be cheap, one time use cartridges for pathogen detection. A schematic of these devices is shown in Figure 27.

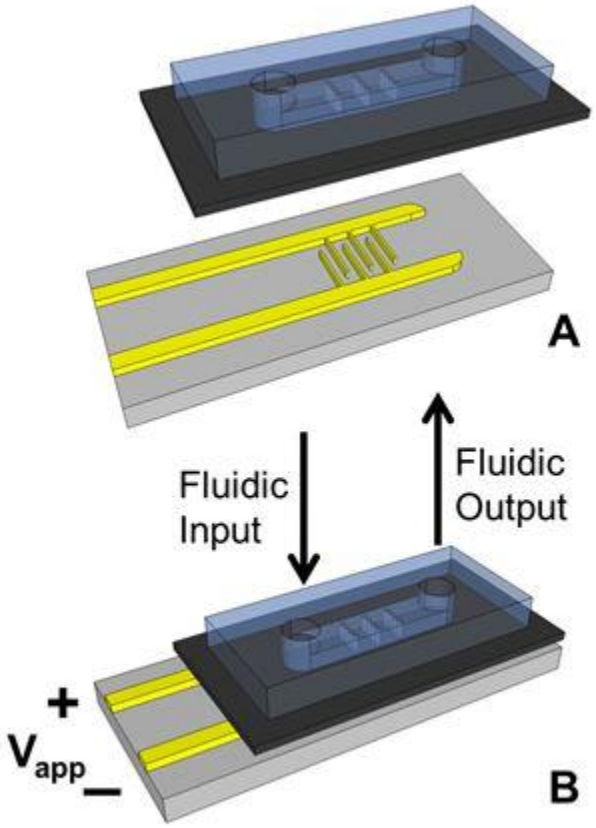

Figure 27 Schematic of OπDEP devices, utilizing a removable cartridge approach

The devices were designed similarly to the EπDEP devices, with only a few differences. Instead of plasma bonding the PDMS device with the channels directly to the glass slide with the electrodes, the PDMS device was instead bonded to a thin glass cover slide, shown in black in Figure 27. The electrodes would then be reusable for different OπDEP devices.

C. Citations of Copyrighted Works

Fig 1 [fair use]
Pruss-Ustun, Annette, R. Bos, F. Gore, J. Bartram. "Safer Water, Better Health: Costs, benefits, and sustainability of interventions to protect and promote health." *World Health Organization*, Geneva, 2008. http://whqlibdoc.who.int/publications/2008/9789241596435_eng.pdf Fair use determination attached.

Fig 3 [fair use]
Srivastava, Soumya K, A. Gencoglu, A. R. Minerick. "DC insulator dielectrophoretic applications in microdevice technology: a review." *Analytical and Bioanalytical Chemistry*. 2010. Fair use determination attached.

Fig 10 [fair use]
Voldman, Joel. "Electrical Forces for Microscale Cell Manipulation." *Annual Review of Biomedical Engineering*. 2006. Fair use determination attached.

Fig 11 [fair use]
Pethig, Ronald. "Review Article – Dielectrophoresis: Status of the theory, technology, and applications." *Biomicrofluidics.* 2010. Fair use determination attached.

Fig 12 [fair use]
Castellarnau, M, A. Errachid, C. Madrid, A. Juarez, J. Samitier. "Dielectrophoresis as a Tool to Characterize and Differentiate Isogenic Mutants of Escherichia coli" *Biophysical Journal*. 2006. Fair use determination attached.

Fig 23 [fair use]
Lewpiriyawong, N. C. Yang. "AC-dielectrophoretic characterization and separation of submicron and micron particles using sidewall AgPDMS electrodes." *Biomicrofluidics*. 2012. Fair use determination attached.